Braz J Phys (2015) 45:621–632
DOI 10.1007/s13538-015-0365-4

SOCIEDADE BRASILEIRA DE FÍSICA

CONDENSED MATTER

Vibrational Spectroscopic and Structural Investigations of 2-Amino-6-Methoxy-3-Nitropyridine: a DFT Approach

S. Premkumar[1] · T. N. Rekha[2] · Beulah J. M. Rajkumar[2] · R. Mohamed Asath[1] · A. Jawahar[3] · T. Mathavan[1] · A. Milton Franklin Benial[1]

Received: 17 June 2015 / Published online: 8 September 2015

Abstract The conformational analysis of 2-amino-6-methoxy-3-nitropyridine molecule (AMNP) has been carried out using density functional theory calculations. The vibrational spectra of the molecule is simulated theoretically and compared experimentally, and the vibrational frequencies are assigned on the basis of potential energy distribution calculations. Electronic properties of the molecule derived from the theoretical ultraviolet–visible spectrum are validated experimentally. The higher non-linear optical activity of the molecule is indicated in the first-order hyperpolarizability calculations. The natural bond orbital and Mulliken atomic charge distribution analysis confirm intramolecular charge transfers and intramolecular interactions. The Frontier molecular orbitals are plotted, and the related molecular properties are calculated and discussed. The molecular electrostatic potential contour map is simulated. As the presence of intramolecular interactions and the associated charge transfers between the pyridine ring of AMNP molecule and the lone pair of oxygen is a common molecular feature of a pharmaceutical compound, this investigation paves the way for its possible biomedical applications. Further, the considerably higher nonlinear optical (NLO) activity of the molecule identified suggests its potential applications in the design of new optical materials.

✉ A. Milton Franklin Benial
miltonfranklin@yahoo.com

[1] Department of Physics, N.M.S.S.V.N. College, Nagamalai, Madurai 625 019, Tamil Nadu, India

[2] Department of Physics, Lady Doak College, Madurai 625 002, Tamil Nadu, India

[3] Department of Chemistry, N.M.S.S.V.N. College, Madurai 625 019, Tamil Nadu, India

Keywords 2-Amino-6-methoxy-3-nitropyridine · Vibrational spectral analysis · UV–vis spectral analysis · Density functional theory studies · Natural bond orbital analysis · Frontier molecular orbitals analysis

1 Introduction

Heterocyclic compounds are of recent scientific interest mainly because of their extensive pharmaceutical, biological, commercial, and industrial applications. Organic aromatic heterocycles containing nitrogen that is derived by replacing a ring carbon atom with a nitrogen atom, are of paramount importance as they are established to have distinct physiochemical properties [1, 2]. Pyridine is a heterocyclic organic compound, structurally related to benzene but with a C–H moiety replaced by a nitrogen atom. It is of utmost utilitarian significance as it is widely used in the synthesis of several organic products, pharmaceuticals, drugs, and agrochemical compounds [3, 4]. Pyridine and its derivatives also exhibit antimicrobial, antifungal, antibacterial, and antitumor properties. The protonation of pyridine is easier due to the presence of the nitrogen atom. The organic non-linear optical (NLO) materials are widely used in optical devices, such as optical switches, optical modulators, optical communications, and optical data storages. Pyridine and its derivatives exhibit NLO properties because of their lone pair of electrons and aminopyridine nitro derivatives have recently been established to be the building blocks of NLO materials. 2-Adamantylamino-5-nitropyridine crystal exhibits large optical non-linearity [5]. 2-(2′-Thienyl)pyridine metal complexes have a wide range of applications in solar energy conversion devices [6]. The pyridine derivatives are also used as color materials due to their unusual electronic properties and their availability in wide ranges of colors. The 2,6-bis(4-carboxyquinolin-2-yl)pyridine complex with ruthenium(II)–polypyridyl complex

(1a) have significant light-harvesting properties in the near-IR region [7]. Recently, several vibrational spectroscopic investigations have been carried out on pyridine derivatives to derive their structural information and vibrational modes [8, 9]. Density functional theory (DFT) methods are employed to compute the molecular structure properties, vibrational frequencies, and energies of the molecular systems. The DFT calculations are also established to correlate well with the experimental spectroscopic techniques such as Fourier transform-infrared (FT-IR), Fourier transform-Raman (FT-Raman), ultraviolet–visible (UV–vis), and nuclear magnetic resonance (NMR) [10, 11]. The spectroscopic techniques combined with the DFT calculations have been proven to be effective in analyzing the functional groups of drugs, tissues, biological fluids, and functional and NLO materials. The influence of molecular structure on the stability and reactivity of the molecules has been drawing attention of many researchers in the recent years. Particularly, the vibrational and UV–vis spectral analysis combined with DFT calculations of pyridine derivatives is greatly focused because of their pharmaceutical and material science applications [12–15].

2-Amino-6-methoxy-3-nitropyridine (AMNP) is a trisubstituted pyridine derivative, with two C–H moieties. The aminopyridine derivatives are used for nucleophilic catalysis in a wide range of asymmetric chiral synthetic processes. The 4-amino pyridine derivative with t-butyl carbomide is used as potential treatments for neurological injury and disease. The 4-aminopyridine acts as a potassium channel blocker, which is capable of restoring conduction in the injured spinal cord. The picoline derivatives prepared from amino pyridine derivatives, which have cholesterol-lowering properties. The derivatives of picoline have potent hypolipidemic effects, anti-neoplastic and anti-inflammatory activities, and show good activity against leukemia and human glioma cell growth [3, 4]. The aminopyridine derivatives serve as a good anesthetic agent and hence they are used in the preparation of drugs for certain brain diseases such as Alzheimer's disease and Lambert-Eaton myasthenia syndrome (LEMS) [3, 4]. In the present investigation, the most stable global minimum molecular structure of 2-amino-6-methoxy-3-nitropyridine is predicted based on the conformation analysis. The vibrational and UV–vis spectra are simulated theoretically and are further validated based on the experimentally recorded spectra as well. The first-order hyperpolarizability, natural bond orbital (NBO) analysis, and frontier molecular orbitals (FMOs) are performed using a DFT calculation.

2 Materials and Methods

2.1 Experimental

The AMNP sample with 99 % purity was purchased from Sigma Aldrich Chemical Co, St. Louis, Mo, USA and was crystallized by slow evaporation method using ethanol as a solvent. FT-IR spectrum was recorded using FT-IR Spectrophotometer (8400S Shimadzu) by a KBr pellet technique at room temperature with a resolution of 4 cm^{-1} using 20 scans. Raman spectrum was recorded using FT-Raman spectrometer (Bruker RFS 27) using Nd/YAG laser wavelength of 1064 nm with a resolution of 2 cm^{-1} at room temperature. The FT-IR and FT-Raman spectra were recorded in the wavenumber region of 3500–400 cm^{-1}. UV–vis spectrum of the molecule was observed using the UV–vis spectrophotometer (UV-2600) in the wavelength region of 200–450 nm, using ethanol as a solvent.

2.2 Computational Details

The conformational analysis was carried out for the AMNP molecule by DFT/B3LYP [16–18] method with 6-31G (d,p) basis set using Gaussian 09 [19] program. The possible conformers of the molecule and global minimum molecular structure were predicted by the potential energy surface (PES) scan. The PES scan was performed at the DFT/B3LYP level of theory with 6-31G (d,p) basis set, varying the torsion angle of 1N-6C-8O-9C in steps of 10° from 0° to 360°. The global minimum molecular structure of the molecule was optimized by the DFT/B3LYP method with 6-311G (d,p), 6-311++G (d,p), and cc-pVTZ basis sets on an Intel core i5/3.10 GHz processor. The vibrational spectra were simulated for the optimized molecular structure of the AMNP molecule by the DFT/B3LYP method with cc-pVTZ basis set. The vibrational modes were assigned on the basis of potential energy distribution (PED) calculations using VEDA 4.0 [20] program. The corresponding vibrational spectra were visualized using GaussView 05 program [21]. The UV–vis spectrum of the AMNP molecule was simulated by the time-dependent (TD)-DFT/B3LYP method associated with the polarizable continuum model (PCM) using cc-pVTZ basis set by choosing ethanol as a solvent. In the PCM model, the ethanol solvent was treated as a continuum dielectric medium and the AMNP molecule was considered as a solute in a cavity surrounded by the ethanol. Mulliken atomic charge distribution, molecular electrostatic potential (MEP) surface contour map, and total electron density mapped with electrostatic potential surface were also derived. The first-order hyperpolarizability was calculated. NBO calculations were performed using NBO 3.1 program [22] as implemented in Gaussian 09. The FMOs were simulated, and the parameters such as the ionization energy, electron affinity, chemical potential, global hardness, and electrophilicity were calculated for the molecule based on Koopman's theorem [23]. All the calculations were done at the ground state energy level of the AMNP molecule without applying any constraints on the potential energy surface. The Raman scattering activities (S_i) of the fundamental modes are suitably converted to

relative Raman intensities (I_i) using the following relationship [24],

$$I_i = \frac{f(\nu_o - \nu_i)^4 S_i}{\nu_i[1-\exp(-hc\nu_i/kT)]}$$

where, ν_0 is the exciting frequency (cm^{-1}), ν_i is the vibrational wavenumber of the *i*th normal mode, h, c, and k are universal constants, and f is the suitably chosen common scaling factor for all the peak intensities.

3 Results and Discussions

3.1 Conformational and Molecular Geometry Analysis

The conformational analysis was carried out to predict the most stable molecular structure of the AMNP molecule. The PES curve of the molecule derived is presented in Fig. 1. Three possible conformers of AMNP molecules were identified and are shown in Fig. 2. PES (Fig. 1.) indicates the stability of the conformers to be in the order of conformer-I> conformer-III>conformer-II, which further suggests that the conformer-I is the most stable molecular structure of the molecule. The conformer-I and conformer-III have planar structures. The conformer-I has the higher stability as compared with that of the conformer-III, and the corresponding relative energy is in the order of 3.10 kcal/mol. The molecular structure of the conformer-III is located at the saddle point of the PES curve. The conformer-II corresponds to the transition state structure of the molecule and has lower stability due to its non-planar molecular structure [3, 25]. The optimized molecular structure of the AMNP molecule was predicted by optimizing the structure of the conformer-I with DFT/B3LYP method using 6-311G (d,p), 6-311++G (d,p), and cc-pVTZ basis sets. Calculated energies of the molecule with three different basis sets are listed in Table 1. The global minimum energy of the molecule was derived using a DFT/B3LYP method with cc-pVTZ basis set. The molecular structure of the AMNP molecule and optimized structure of the AMNP molecule are shown in Fig. 3. The calculated vibrational frequencies of the optimized molecular structure of the AMNP molecule have only positive values confirming that the optimized geometry is located at the local minimum on the potential energy surface. Figure 3 indicates the formation of an intramolecular hydrogen bond between the 11H-18O and 16H-19O atoms after the optimization, leading to the higher stability of the molecule [3, 4].

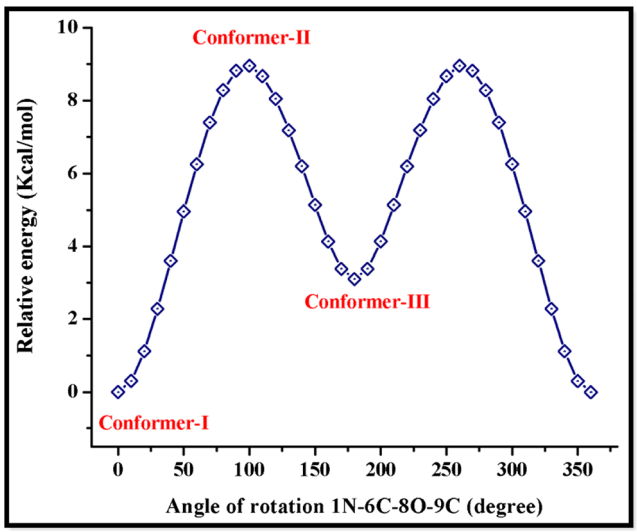

Fig. 1 The potential energy surface profile of the AMNP molecule

3.2 Mulliken Atomic Charge Distribution Analysis

Mulliken atomic charge distribution is useful in describing the intramolecular charge transfers (ICT) of the molecular systems. The electronic charges derived from Mulliken atomic charge distribution analysis of the AMNP molecule are indicated in Fig. 4. The intramolecular hydrogen bond formation is indicated between the most positive and most negative atoms, confirming the presence of intramolecular charge transfers between the corresponding atoms. This ICT accounts for the higher stability of the molecule and the enhancement in NLO and bioactivity of the molecule [4]. Calculated total Mulliken atomic charge for AMNP molecule is zero. The most positive (7N) and most negative (19O) atoms are part of the nitro group. In the nitro group, the electronegative nitrogen atom (7N) is of the highest positive charge and behaves as an electron acceptor in the presence of the more electronegative oxygen atoms (19O and 18O). In methoxy group, hydrogen atoms (13H, 14H, and 15H) have positive charge values, and the oxygen atom (8O) is negatively charged leaving the 6C carbon atom positive [3, 4]. All the hydrogen atoms of the AMNP molecule have positive charge values, whereas the carbon atoms have positive as well as negative charge values. This further confirms the presence of ICT within the molecule through the carbon atoms [3, 4]. The intramolecular hydrogen bond formation between 19O-16H and 18O-11H atoms can be correlated to the strong electrostatic interaction between the electro-negative atoms (19O and 18O) and electro-positive atoms (16H and 11H).

3.3 Vibrational Spectral Analysis

The AMNP molecule has 19 atoms and 51 normal modes of vibrations which belong to the same symmetry species (A). The molecule possesses C_1 point group symmetry implying that all the vibrational modes of AMNP molecule are both infrared (IR) and Raman active. The vibrational coordinates such as vibrational frequencies, infrared intensity, Raman activity, reduced mass, and force constant of AMNP molecule

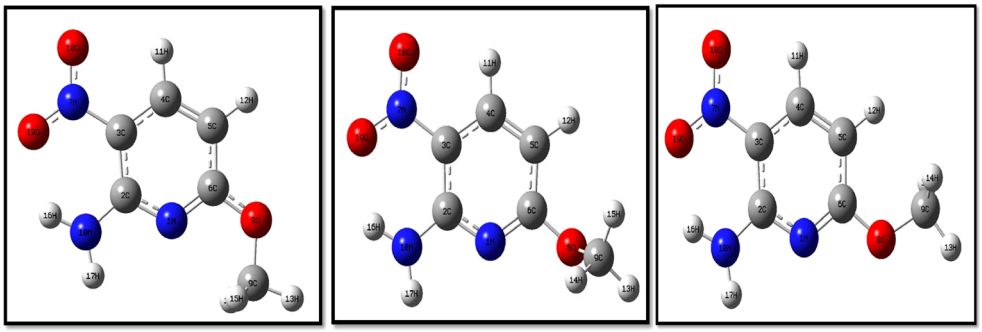

Fig. 2 The possible conformers of the AMNP molecule with corresponding relative energy and angle of rotation between the torsion angle of 1N-6C-8O-9C

were calculated. Theoretical vibrational frequencies were scaled in order to account for the anharmonicity in DFT calculations [26]. The different scaling factors were used for different ranges of calculated vibrational modes for establishing better agreement with the experimental values. The scaling factors of the AMNP molecule were calculated using the formula [3, 4],

$$C = \frac{\sum \left(\gamma_i * \omega_i\right)}{\sum \omega_1^2}$$

Where, C is the scaling factor, γ_i and ω_i are experimental fundamental frequency, and theoretical harmonic frequency, respectively. The calculated scaling factors of bending, stretching and NH_2 stretching vibrations are 0.9916, 0.9730, and 0.9391, respectively. The vibrational modes of experimental and theoretical values and their assignments are listed in Table 2. Experimental and theoretical infrared and Raman spectra of the AMNP molecule are provided in Figs. 5 and 6.

3.3.1 Ring C–H Vibrations

The pyridine and its derivatives exhibit multiple weak bands in the region 3100–3000 cm^{-1}, which are assignable to the C–H stretching vibrations [27, 28]. The AMNP molecule is a trisubstituted pyridine derivative, with two C–H moieties. These C–H moieties give rise to two stretching vibrations: asymmetric and symmetric C–H stretching vibrations. The calculated C–H asymmetric and symmetric stretching vibrations in the current study of the AMNP molecule were identified at 3143 and 3131 cm^{-1}, respectively. The corresponding asymmetric stretching modes were observed experimentally at 3104 cm^{-1} in FT-IR and 3105 cm^{-1} in FT-Raman spectra, respectively. Generally, the C–H in-plane bending vibrational modes are in the wavenumber region of 1500–1445 and 1300–1180 cm^{-1}

Table 1 The calculated energies of the AMNP molecule by DFT/B3LYP method with 6-311G (d,p), 6-311++G (d,p), and cc-pVTZ basis sets

Basis sets	Energy (a.u.)
cc-pVTZ	−622.92855
6-311++G (d,p)	−622.87856
6-311G (d,p)	−622.86223

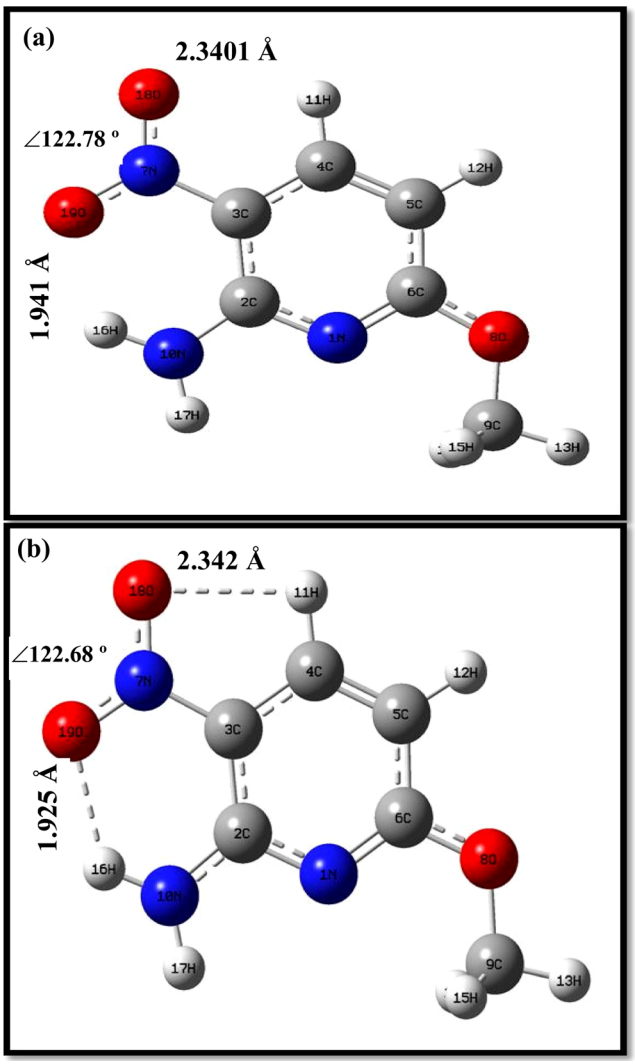

Fig. 3 The optimized molecular structure of AMNP molecule **a** before optimization and **b** after optimization

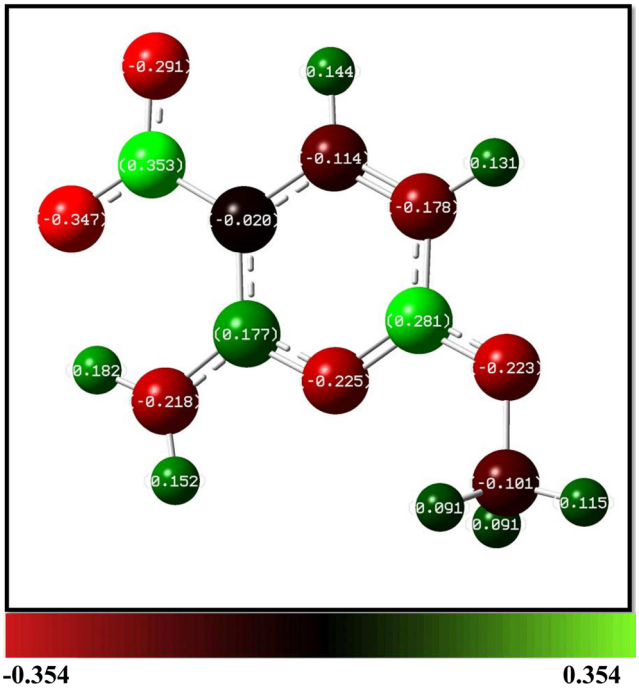

Fig. 4 The Mulliken atomic charge distribution of AMNP molecule

[27]. In AMNP molecule, the calculated C–H in-plane bending vibrational modes coupled with methyl asymmetrical and NH_2 in-plane bending vibrational modes were identified at 1499 and 1452 cm^{-1}, respectively. The corresponding vibrational modes were observed at 1493 cm^{-1} in FT-IR spectrum. The C–H rocking vibrational modes of the AMNP molecule coupled with ring stretching vibrational mode were calculated at 1273 cm^{-1} and were observed at 1244 cm^{-1} in FT-IR and 1234 cm^{-1} in FT-Raman spectra, respectively, which indicates that the hydrogen bond has strong impact on the positions of the vibrational levels. The C–H scissoring vibrational modes of the AMNP molecule were predicted at 1170 and 1089 cm^{-1}. The corresponding vibrational modes were observed at 1094 and 1070 cm^{-1} in FT-IR and FT-Raman spectra, respectively. In AMNP molecule, the calculated C–H out-of-plane bending vibrational modes are at 994, 823, and 743 cm^{-1}. Experimentally, the C–H out-of-plane bending vibrations of the AMNP molecule were observed at 995, 820, and 733 cm^{-1} in FT-IR spectrum and at 999 and 735 cm^{-1} in FT-Raman spectrum. These assignments agree well with the literature values [3, 4, 12].

3.3.2 Ring C–C Vibrations

In aromatic compounds, the ring C–C stretching vibrations are highly characteristic vibrational modes and are usually recorded with varying intensities in the wavenumber region of 1635–1100 cm^{-1} [27, 29]. In the case of the AMNP molecule, the calculated ring C–C stretching vibrational modes were coupled with various stretching and bending vibrational modes as well and were identified in the wavenumber range of 1610–1500 and 1380–1270 cm^{-1}. These rings C–C stretching vibrational modes of the AMNP molecule were experimentally observed at 1614, 1564, 1366, and 1244 cm^{-1} in FT-IR spectrum and at 1601, 1570, 1362, 1334, and 1196 cm^{-1} in FT-Raman spectrum. Further, in the FT-IR spectrum, the peaks observed at 1614 and 1244 cm^{-1} were much broader. The broadening of the peaks can be attributed to the presence of C–C conjugative and ICT interactions along with the coupling vibrational modes such as ring C–C and C–N stretching, NH_2 in-plane bending, C–H in-plane bending and C–NH_2 stretching vibrations [8, 12, 13].

3.3.3 Ring C–N Vibration

Aromatic ring C–N stretching vibrational modes with varying intensities are documented in the wavenumber region of 1590–1520, 1480–1400, 1410–1375, 1350–1250, and 1270–1065 cm^{-1} [27, 29]. In AMNP molecule, the calculated ring C–N stretching vibrational modes coupled with other vibrations, as listed in Table 2, were identified at 1606, 1503, 1379, and 1089 cm^{-1}. The FT-IR peaks at 1614, 1366, and 1094 cm^{-1} and the FT-Raman peaks at 1601 and 1070 cm^{-1}, were assigned to the ring C–N stretching vibrations of the AMNP molecule. These assignments also correlate well with the reported literature values [3, 11, 12].

3.3.4 Ring Breathing Mode

The pyridine ring breathing vibrational modes are sensitive to the mass and position of the substitution and are normally present in the wavenumber region of 900–750 cm^{-1} [30]. In AMNP molecule, pyridine ring vibration was calculated at 964 cm^{-1} and the corresponding vibrational mode was experimentally observed at 951 cm^{-1} in the FT-IR spectrum [12]. The calculated and observed ring in plane and out-of-plane bending vibrational modes and skeletal vibrations were assigned and listed in Table 2.

3.3.5 NH_2 and C–NH_2 Vibrations

The electron donating amino group (NH_2) substituted in the aromatic ring system has six internal modes of vibrations. These vibrational modes are asymmetric stretching, symmetric stretching, scissoring, rocking, wagging and torsion. The NH_2 asymmetric and symmetric stretching vibrational modes generally appear in the wavenumber ranges of 3450–3330 and 3300–3250 cm^{-1} [27, 28]. The asymmetric and symmetric stretching vibrational modes of the AMNP molecule were calculated at 3489 and 3343 cm^{-1}, respectively, and the corresponding vibrational modes were observed at 3476 and 3346 cm^{-1} in FT-IR spectrum. The NH_2 symmetrical stretching vibrational mode was observed at 3356 cm^{-1} in FT-Raman spectrum. In AMNP molecule, the calculated

Table 2 The observed, calculated vibrational wavenumber (cm^{-1}), infrared intensity (km mol^{-1}), Raman scattering activity ($Å^4$ amu^{-1}), reduced mass (amu), force constant (mDyne/$Å^{-1}$), and vibrational assignments based on the PED for the AMNP molecule

Serial no.	Wavenumber (cm^{-1})				Infrared intensity	Raman activity	Reduced mass	Force constant	Assignment with PED%
	Unscaled	Scaled	FT-IR	FT-Raman					
1.	3715	3489	3476 vs		94.61	46.73	1.10	8.98	ν_{as} NH_2 (99)
2.	3560	3343	3356 vs	3356 vw	85.09	131.15	1.05	7.81	ν_s NH_2 (99)
3.	3230	3143			2.32	121	1.10	6.74	ν_s Φ CH (99)
4.	3217	3131	3104 m	3105 w	0.9	52.8	1.09	6.64	ν_{as} Φ CH (100)
5.	3149	3064		3036 w	18.22	111.35	1.11	6.46	ν_{as} CH_3 (98)
6.	3115	3031	2992 vw	2992 vw	20.71	45.46	1.11	6.33	ν_{as} CH_3 (98)
7.	3047	2965	2955 vw	2955 w	40.19	178.25	1.03	5.63	ν_s CH_3 (99)
8.	1650	1606	1614 vs (b)	1601 w	565.02	13.1	6.76	10.84	ν Φ C=C (33), ν 2C-10N (11), ν Φ C=N (10), δ NH_2 (10)
9.	1629	1585	1564 w	1570 w	386.75	13.01	4.57	7.14	ν Φ C=C (34), δ NH_2 (16), ν 19O-16H (13), ν C–NH_2 (10)
10.	1593	1550			45.45	10.45	2.09	3.12	δ NH_2 (47), ν_{as} NO_2 (33)
11.	1545	1503			74.47	7	7.91	11.12	ν_{as} NO_2 (37), ν Φ C=N (18), ν Φ C=C (15)
12.	1512	1499	1493 w		94.14	3.87	2.10	2.83	β_{as} CH_3 (31), β Φ CH (17), ν 6C-8O (16)
13.	1501	1488			24.39	6.04	1.08	1.43	β_{as} CH_3 (82)
14.	1485	1473	1466 s	1461 w	8.62	12.26	1.05	1.36	β_{as} CH_3 (98)
15.	1464	1452		1437 w	150.99	2.95	2.14	2.70	δ NH_2 (23), β Φ CH (18), ν_{as} NO_2 (15), ν C–NH_2 (14)
16.	1455	1443	1414 m	1415 m	53.6	20.87	1.85	2.31	β_{as} CH_3 (49)
17.	1391	1379	1366 m	1362 vs	207.88	103.87	5.05	5.76	ν Φ C=N (54), ν Φ C=C (24), β_s CH_3 (12)
18.	1356	1345		1334 vs	20.51	131.36	7.83	8.48	ν Φ C=C (36), ν_s NO_2 (25).
19.	1302	1291			870.16	118.61	7.66	7.65	ν_s NO_2 (34), ν Φ C=C (26), β_s CH_3 (15)
20.	1284	1273	1244 w (b)	1234 vs	12.34	2.88	2.00	1.94	ρ Φ CH (32), ν Φ C=C (14), ν 6C-8O (13), ν C–NH_2 (12)
21.	1221	1211		1196 w	8.04	2.53	1.59	1.40	ρ CH_3 (66)
22.	1179	1170			12.41	3.32	1.74	1.42	δ Φ CH (51), ρ CH_3 (18)
23.	1175	1165	1161 vw	1164 w	0.82	1.98	1.27	1.03	ρ CH_3 (98)
24.	1121	1112	1132 w	1136 w	48.73	25.39	2.44	1.81	ρ NH_2 (28), β Φ C=C (21), ν C–NO_2 (17)
25.	1099	1089	1094 w	1070 w	75.44	3.02	1.99	1.41	δ Φ CH (40), ν Φ C=N (18).
26.	1031	1022			53.98	5.14	4.90	3.07	ν O–CH_3 (66)
27.	1003	994	995 m	999 m	1.08	0.28	1.31	0.78	η Φ CH (83)
28.	972	964	951 vw		5.59	0.48	3.04	1.69	Ring breathing mode
29.	856	849		836 s	12.58	29.41	9.57	4.13	δ NO_2 (62)
30.	830	823	820 s		23.82	0.32	1.91	0.78	η Φ CH (65), η Φ C–C (13)
31.	799	792	775 s		30.07	0.7	9.53	3.59	ω Φ (54), ω NO_2 (32)
32.	751	744			0.13	14.42	6.10	2.02	β Φ C–C–C (40)
33.	750	743	733 w	735 w	5.34	0.12	5.03	1.67	ω NO_2 (49), η Φ CH (22)
34.	708	702	693 vw		1.32	0.02	3.01	0.89	ω NH_2 (40), ω Φ (32)
35.	668	662	656 s	660 vw	13.49	2.81	5.91	1.55	γ skeletal (53)
36.	659	653		647 vw	2.54	0.7	1.12	0.29	ω NH_2 (77)
37.	595	590	588 m	590 w	4.79	9.96	5.91	1.23	γ skeletal (61)
38.	562	557	552 w	555 vw	11.29	4.09	5.30	0.99	γ Φ (48)
39.	503	499	503 m	498 w	6.59	0.3	5.84	0.87	β 6C-8O-9C (40), ρ NO_2 (25)
40.	463	459		448 vw	1.87	1.01	3.76	0.47	τ Φ (67)
41.	404	400	417 w	421 w	6.56	4.98	4.18	0.40	β 3C-2C-10N (52)
42.	352	349			2.76	2.79	7.21	0.53	β group (67)
43.	325	323			120.41	0.65	1.55	0.10	τ NH_2 (66)

Table 2 (continued)

Serial no.	Wavenumber (cm^{-1})				Infrared intensity	Raman activity	Reduced mass	Force constant	Assignment with PED%
	Unscaled	Scaled	FT-IR	FT-Raman					
44.	289	287			5.69	4.56	5.79	0.29	β group (73)
45.	280	278			52.51	0.51	2.45	0.11	η Φ (44), τ NH_2 (28)
46.	223	221			0.01	0.23	5.11	0.15	η skeletal (63)
47.	193	192			1.63	1.24	3.92	0.09	β group (67)
48.	170	169			0.14	0.45	1.31	0.02	η CH_3 (75)
49.	146	144			3.01	0.32	2.69	0.03	η CH_3 (74)
50.	81	81			0.5	0.03	12.39	0.05	η NO_2 (79).
51.	66	65			0.02	0.05	5.08	0.01	Butterfly mode

vs very strong, *s* strong, *m* medium, *w* weak, *vw*very weak, *b* broad, *Φ* ring, *ν* stretching, ν_{as} asymmetrical stretching, ν_s symmetrical Stretching, *η* out-of-plane bending, *β* in-plane bending, β_s symmetrical in-plane bending, β_{as} asymmetrical in-plane bending, *δ* scissoring, *ρ* rocking, *ω* wagging, *τ* torsion, *t* twisting, *γ* deformation

NH_2 scissoring vibrational modes coupled with the ring stretching and C–NH_2 stretching vibrational modes were noticed at 1614, 1585, 1550, and 1452 cm^{-1} and the corresponding vibrational modes were observed at 1614 and 1564 cm^{-1} in FT-IR and 1601 and 1570 cm^{-1} in FT-Raman spectra. The NH_2 rocking vibrational modes of the AMNP molecule were calculated at 1112 cm^{-1}, and the corresponding vibrational modes were observed at 1132 cm^{-1} in FT-IR and 1136 cm^{-1} in FT-Raman spectra, respectively. In AMNP molecule, the wagging vibrational modes were calculated at 702 and 653 cm^{-1} and were observed at 693 cm^{-1} in FT-IR spectrum and 647 cm^{-1} in FT-Raman spectrum [11, 31].

The calculated C–NH_2 stretching vibrational modes of the AMNP molecule were identified at 1585 and 1452 cm^{-1} but were accompanied with NH_2 scissoring vibrations as well. Whereas, the calculated peak at 1273 cm^{-1} assigned to the C–NH_2 stretching vibration was without the contribution of NH_2 scissoring vibration but was coupled with the ring stretching and C–H rocking vibrations. The corresponding vibrational mode was experimentally observed at 1244 cm^{-1} in FT-IR and 1234 cm^{-1} in FT-Raman spectra. These assignments correlate well with the literature values reported [8, 12].

3.3.6 NO_2 and C–NO_2 Vibrations

The electron withdrawing nitro group (NO_2) contributes to six normal modes of vibrations, such as asymmetric stretching, symmetric stretching, scissoring, rocking, wagging, and out-of-plane bending vibrations. The asymmetric and symmetric NO_2 stretching vibrations of aromatic compounds generally occur in the wavenumber regions of 1570–1485 and 1370–1320 cm^{-1} [28, 29]. The calculated NO_2 asymmetric stretching vibrational modes coupled with certain other vibrational modes were identified at 1550, 1503, and 1452 cm^{-1}. The corresponding vibrational modes were observed at 1437 cm^{-1} in FT-Raman spectrum. The NO_2 symmetric stretching vibrational modes were calculated at 1345 and 1291 cm^{-1} and were experimentally recorded at 1334 cm^{-1} in FT-Raman spectrum. In general, scissoring vibration of NO_2 occurs in the wavenumber region of 890–830 cm^{-1}. In

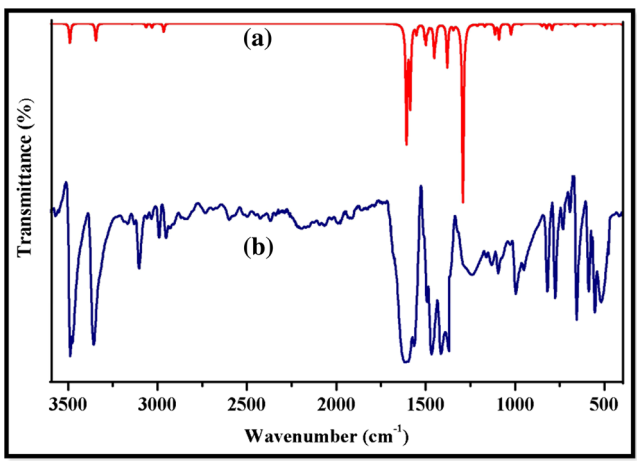

Fig. 5 The infrared spectra of AMNP molecule: **a** theoretical and **b** experimental

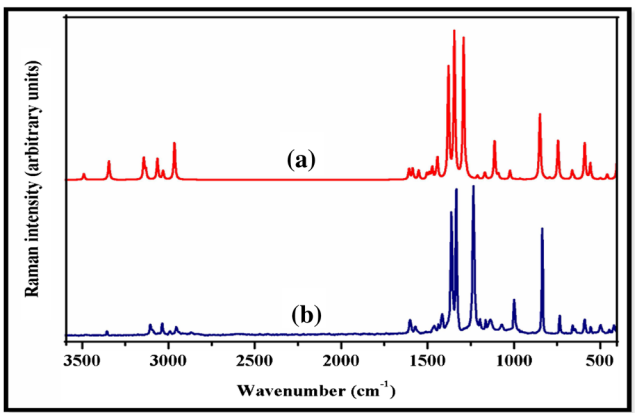

Fig. 6 The Raman spectra of AMNP molecule: **a** theoretical and **b** experimental

AMNP molecule, the calculated NO_2 scissoring vibration was obtained at 849 cm^{-1} and the corresponding vibrational mode was observed at 836 cm^{-1} in FT-Raman spectrum. The calculated NO_2 wagging vibrational modes coupled with ring wagging and ring C–H out-of-plane bending vibrations were identified at 792 and 743 cm^{-1} and the corresponding vibrational modes were observed experimentally at 775 and 733 cm^{-1} in FT-IR spectrum and at 735 cm^{-1} in FT-Raman spectrum. The NO_2 rocking vibration of the AMNP molecule was calculated at 499 cm^{-1}. The corresponding vibrational mode was observed at 503 cm^{-1} in FT-IR and 498 cm^{-1} in FT-Raman spectrum, respectively. These assignments also agree well with the literature values [12, 31]. The calculated NO_2 out-of-plane bending vibration was identified in the lower wavenumber region. Hence, the corresponding vibrational mode was not experimentally observed. The calculated peak at 1112 cm^{-1} contributes to the C–NO_2 stretching vibration and was experimentally observed at 1132 cm^{-1} in FT-IR spectrum and at 1136 cm^{-1} in FT-Raman spectrum. This assignment also correlates well with the literature values [8, 12].

3.3.7 CH_3 and O–CH_3 Vibrations

When the electron donating methyl (CH_3) group is directly attached to an oxygen atom, the C–H stretching and bending bands can shift energetically due to the associated electronic effects. This causes a spread of O–CH_3 stretching vibrational bands over a larger region than that of the C–CH_3 group. The asymmetric and symmetric CH_3 stretching vibrations of the methoxy group are generally reported in the wavenumber region of 3000–2815 cm^{-1} [29, 30]. In AMNP molecule, the calculated asymmetric stretching vibrational modes were identified at 3064 and 3031 cm^{-1} and corresponding vibrational modes were observed at 2992 cm^{-1} in FT-IR spectrum and at 3036 and 2992 cm^{-1} in FT-Raman spectrum. The symmetric stretching vibration was calculated at 2965 cm^{-1} and was observed at 2955 cm^{-1} in both FT-IR and FT-Raman spectrum. The calculated asymmetric in-plane bending vibrations of methoxy group was noticed in the region, 1500–1440 cm^{-1}. The observed peaks at 1493, 1466, and 1414 cm^{-1} in FT-IR spectrum and at 1461 and 1414 cm^{-1} in FT-Raman spectrum were assigned to the asymmetric in-plane bending vibrations of the AMNP molecule. The CH_3 symmetric in-plane bending vibrations of the molecule were calculated at 1379 and 1291 cm^{-1}, and the corresponding vibrational modes were observed at 1366 cm^{-1} in FT-IR spectrum and at 1334 cm^{-1} in FT-Raman spectrum. The calculated CH_3 rocking vibrations of the AMNP molecule were noticed at 1211, 1170, and 1165 cm^{-1}. The corresponding CH_3 rocking vibrational modes were experimentally observed at 1161 cm^{-1} in FT-IR spectrum and 1196 and 1164 cm^{-1} in FT-Raman spectrum, respectively. These assignments agree well with the literature values [11, 32]. The CH_3 out-of-plane bending vibration was calculated in the range of 280–210 cm^{-1}. Hence, the corresponding vibrational mode was not experimentally observed. Normally, the C=O and C–O stretching vibrations are present in the frequency ranges of 1770–1650 and 1260–1000 cm^{-1}, respectively [28, 29]. In AMNP molecule, C–O stretching vibrations were calculated at 1499 and 1273 cm^{-1} and were observed at 1499 and 1244 cm^{-1} in FT-IR spectrum and at 1234 cm^{-1} in FT-Raman spectrum.

3.4 UV–vis Spectral and FMOs Analysis

The electronic properties of the AMNP molecule were further investigated based on UV–vis spectral analysis. The observed and simulated UV–vis spectra of the molecule are presented in Fig. 7, and the corresponding UV–vis parameters are listed in Table 3. In AMNP molecule, two electronic transitions were experimentally observed at 377 and 248 nm with excitation energy values of 3.28 and 5.06 eV, respectively. These peaks can be assigned to the n–π^* and π–π^* transitions, respectively [33, 34]. The n–π^* transitions of the AMNP molecule originate from the ICT interactions between the lone pair electrons of the electronegative atoms and the π electrons present in the aromatic rings. These transitions were calculated at 347 and 307 nm with excitation energy values of 3.57 and 4.05 eV, respectively, and are associated with the respective oscillator strengths of 0.2546 and 0.000. The calculated π–π^* electronic transition of the molecule was identified at 272 nm with 4.55 eV excitation energy and an oscillator strength of 0.001. This transition was experimentally observed at 248 nm. The π–π^* transition of the molecule leaves the molecule as unsaturated compound and subsequently enhances the ICT interactions and intra and intermolecular hydrogen bond formation. This transition is also responsible for the higher NLO activity of the molecule [33, 34]. The UV–vis spectral analysis confirms the presence of more significant n–π^* and π–π^* electronic transitions of AMNP molecule arising out of the

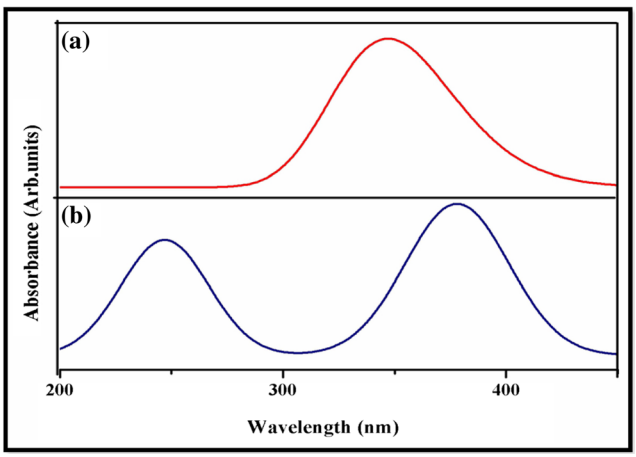

Fig. 7 The UV–vis spectra of AMNP molecule: **a** theoretical and **b** experimental

interactions between the lone pair electrons of the electronegative atoms and the π electrons.

The FMOs are helpful to illustrate the conjugation, aromaticity and lone pairs of aromatic organic molecules. The highest occupied molecular orbital (HOMO) possesses an antibonding character and represents the ability to donate an electron and the lowest unoccupied molecular orbital (LUMO) indicates a bonding character and as an electron acceptor, it represents the ability to receive an electron. The ionization potential (IP), electron affinity (EA), electronegativity (χ), hardness (η), softness (S), chemical potential (μ), and electrophilicity index (ω) are called as global reactivity descriptors and are widely used in describing the reactivity and stability of the chemical systems. The FMOs related molecular properties such as IP, EA, χ, η, S, μ, and ω of the AMNP molecule were further calculated from HOMO and LUMO energies using the formulae [23, 35], $\mathrm{IP} = -E_{\mathrm{HOMO}}$, $\mathrm{EA} = -E_{\mathrm{LUMO}}$, $\chi = \frac{1}{2}(\mathrm{IP} + \mathrm{EA})$, $\eta = \frac{1}{2}(\mathrm{IP}-\mathrm{EA})$, $S = \frac{1}{\eta}$, $\mu = -\frac{1}{2}(\mathrm{IP} + \mathrm{EA})$ and $\omega = \mu^2/2\eta$

The calculated HOMO, LUMO, energy gap, IP, EA, η, μ, and ω values of the AMNP molecule are provided in Table 4. The visualization of FMOs of the molecule as represented in Fig. 8 confirms the presence of delocalized electron density within the molecule. The lower energy gap between HOMO and LUMO of AMNP molecule confirms the charge transfers within the molecule which can be correlated to the ICT and is responsible for the bio and the NLO activity of the molecule. The calculated softness of the molecule is lower, confirming the softness of the molecule. The chemical potential and electrophilicity index values of the AMNP molecule also confirm its higher chemical reactivity [4, 36].

Table 4 The calculated FMOs and related molecular properties of the AMNP molecule

Molecular properties	Energy (eV)
HOMO	−6.48
LUMO	−2.33
$E_{\mathrm{LUMO}}-E_{\mathrm{HOMO}}$	4.15
Ionization potential (IP)	6.48
Electron affinity (EA)	2.33
Electronegativity (χ)	4.41
Hardness (η)	2.08
Softness (S)	0.48
Chemical potential (μ)	−4.41
Electrophilicity index (ω)	4.68

3.5 First-Order Hyperpolarizability Calculation

The first-order hyperpolarizability (β_{tot}) of AMNP molecule was calculated based on the finite field approach. In the presence of an applied electric field, the energy of a system is a function of the electric field. The first-order hyperpolarizability is a third rank tensor, which can be described by a 3×3×3 matrix. The 27 components of the 3D matrix can be reduced to 10 components because of the Kleinman symmetry [37]. The matrix can be given in the lower tetrahedral format, the lower part of the 3×3×3 matrix being a tetrahedral. The components of β are defined as the coefficients in the Taylor series expansion of the energy in the external electric field. When the external electric field is weak and homogeneous, this expansion becomes

$$E = E^0 - \mu_\alpha F_\alpha - \frac{1}{2}\alpha_{\alpha\beta} F_\alpha F_\beta - \frac{1}{6}\beta_{\alpha\beta\gamma} F_\alpha F_\beta F_\gamma + \ldots\ldots$$

where E^0 is the energy of the unperturbed molecules, F_α is the field at the origin, μ_α, $\alpha_{\alpha\beta}$, and $\beta_{\alpha\beta\gamma}$ are the components of the dipole moment, polarizability and first-order hyperpolarizability, respectively. The mean first-order hyperpolarizability (β_{tot}) is calculated using the x-, y-, and z-components as

$$\beta_{\mathrm{tot}} = \sqrt{\left(\beta_x^2 + \beta_y^2 + \beta_z^2\right)}$$

The calculated first-order hyperpolarizability components of the AMNP molecule are listed in Table 5. The first-order hyperpolarizability value, 5.75×10^{-30} esu, of the AMNP molecule confirms its higher NLO activity [4, 36].

3.6 MEP Surface Contour Map Analysis

The MEP surface contour map illustrates the charge distributions of a molecular system two dimensionally and is helpful in determining how the molecule interacts with another. The MEP surface contour map provides information about the reactive sites of the molecule for both electrophilic and nucleophilic reactions [38]. The MEP surface contour map of the AMNP molecule was further plotted with the electron density

Table 3 The calculated and observed UV–vis spectra parameters and its assignments of the AMNP molecule in ethanol solution

Contribution of orbital	Theoretical		f	Experimental		Assignment
	λ (nm)	E (eV)		λ (nm)	E (eV)	
H→L (70 %)	347	3.57	0.2546	377	3.28	n–π*
H-2→L (55 %) H-3→L (41 %)	307	4.05	0.000		n–π*	
H-3→L (40 %) H-5→L (48 %)	272	4.55	0.001	248	5.06	π–π*

λ wavelength, E excitation energies, f oscillator strength

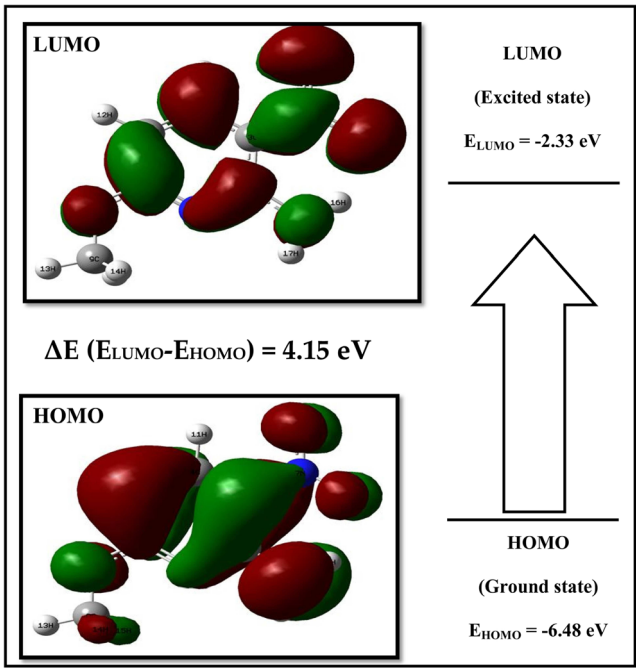

Fig. 8 The HOMO and LUMO orbitals of AMNP molecule

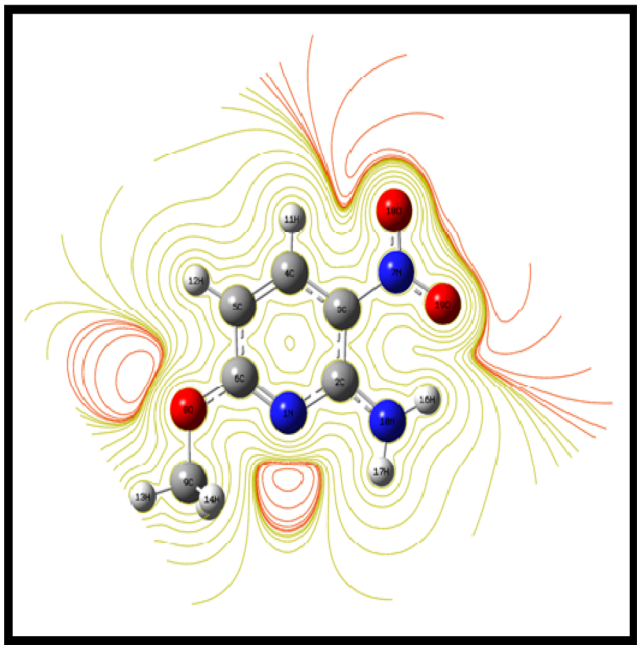

Fig. 9 The molecular electrostatic potential surface contour map of AMNP molecule

isosuface value of 0.02 a.u and is shown in Fig. 8. The red color line in Fig. 9 represents the negative electrostatic potential and a yellow color line indicates the positive electrostatic potential. It is identified that the positive electrostatic region of the AMNP molecule is present over all the atoms around their nuclear position [38]. The negative electrostatic potential is present over the positive electrostatic region of the nitro group, 1N and 8O atoms and are the possible sites for the electrophilic reactions. The positive electrostatic potential over the hydrogen atoms are the possible sites for the nucleophilic reactions.

3.7 Natural Bond Orbital Analysis

NBO analysis is used to investigate the delocalization of electron density due to the ICT of a molecular system.

Table 5 The calculated first-order hyperpolarizability components of the AMNP molecule

β components	Values (a.u.)
β_{xxx}	913.2096
β_{xxy}	−38.0112
β_{xyy}	−210.4839
β_{yyy}	−82.0552
β_{xxz}	−0.0114
β_{xyz}	−0.0094
β_{yyz}	0.0732
β_{xzz}	−43.4815
β_{yzz}	25.3546
β_{zzz}	0.0140
β_{tot}	666.0130

The delocalization of electron density between occupied Lewis type NBO orbital and formally unoccupied non-Lewis NBO orbital corresponds to the stabilizing donor-acceptor interactions leading to the charge transfers or hyperconjugative interactions in the molecular systems [39]. The stabilization energy $E_{(2)}$ associated with the delocalization $i \rightarrow j$ are calculated on the basis of second-order Fock matrix perturbation theory and are estimated for each donor (i) and acceptor (j) by using the following equation

$$E_{(2)} = \Delta E_{ij} = q_i \frac{F^2_{(i,\ j)}}{E_i - E_j}$$

Where, q_i is the donor orbital occupancy, E_i and E_j are the energies of σ and σ^* diagonal elements, and $F_{(i,\ j)}$ is the off-diagonal NBO Fock matrix element.

The important stabilization interactions between the Lewis and non-Lewis orbital of AMNP molecule are listed in Table 6. The strong stabilization interaction is identified between the lone pair of N10 and π^* (C2-C3) causing the lower donor electron density and higher acceptor electron density. This transition leads to the higher electronic oscillator strength at 347 nm in UV–vis spectrum. This interaction also causes the ICT from the lone pair of N10 to the pyridine ring of the AMNP molecule, which is a common molecular feature of a pharmaceutical compound. The similar interaction was identified between the lone pair of O8 to σ^* (C5-C6). This interaction is associated to the ICT occurring between the pyridine ring and the lone pair of O8. Hence, these interactions may lead to the higher bioactivity of the AMNP molecule [40]. In the current investigation of

Table 6 The second-order perturbation theory analysis of Fock matrix in NBO basis of the AMNP molecule

Donor (*i*)	ED (*e*)	Acceptor (*j*)	ED (*e*)	$E_{(2)}$ kcal/mol	$E_{(j)}-E_{(i)}$ a.u.	$F_{(i,j)}$ a.u.
σ (N1-C2)	1.9783	σ* (C6-O8)	0.0490	4.64	1.22	0.07
σ (N1-C6)	1.9888	σ* (C2-N10)	0.0251	3.37	1.33	0.06
π (N1-C6)	1.7777	π* (C2-C3)	0.4797	29.88	0.31	0.09
π (N1-C6)		π* (C4-C5)	0.2593	6.55	0.35	0.04
π (C2-C3)	1.5905	π* (N1-C6)	0.4177	9.22	0.26	0.04
π (C2-C3)		π* (C2-C3)	0.4797	4.95	0.26	0.03
π (C2-C3)		π* (C4-C5)	0.2593	26.21	0.29	0.08
π (C2-C3)		π* (N7-O18)	0.6615	40.41	0.15	0.07
σ (C3-C4)	1.9776	σ* (C2-N10)	0.0252	3.60	1.19	0.06
σ (C3-C4)		σ* (C5-H12)	0.0134	3.09	1.13	0.05
σ (C4-C5)	1.9764	σ* (C3-N7)	0.0988	3.81	1.03	0.06
σ (C4-C5)		σ* (C6-O8)	0.0490	3.74	1.12	0.06
π (C4-C5)	1.7459	π* (N1-C6)	0.4177	30.56	0.26	0.08
π (C4-C5)		π* (C2-C3)	0.4796	10.88	0.26	0.05
σ (C4-H11)	1.9726	σ* (C2-C3)	0.0452	4.88	1.00	0.06
σ (C4-H11)		σ* (C5-C6)	0.0394	4.23	1.03	0.06
σ (C5-C6)	1.9778	σ* (C4-H11)	0.0139	3.26	1.14	0.05
σ (C5-C6)		σ* (O8-C9)	0.0156	4.34	0.96	0.06
σ (C5-H12)	1.9761	σ* (N1-C6)	0.0271	4.67	1.07	0.06
σ (C5-H12)		σ* (C3-C4)	0.0182	4.45	1.03	0.06
π (N7-O18)	1.9886	π* (C2-C3)	0.4797	3.68	0.43	0.04
π (N7-O18)		π* (N7-O18)	0.6613	8.11	0.32	0.05
σ (O8-C9)	1.9906	σ* (N1-C6)	0.0394	3.58	1.32	0.06
σ (C9-H13)	1.9899	σ* (C6-O8)	0.0490	4.31	0.91	0.06
σ (N10-H16)	1.9897	σ* (N1-C2)	0.0184	4.66	1.17	0.07
σ (N10-H17)	1.9884	σ* (C2-C3)	0.0452	5.07	1.15	0.07
LP N1	1.8869	σ* (C2-C3)	0.0452	11.73	0.84	0.09
LP N1		σ* (C2-N10)	0.0252	3.71	0.82	0.05
LP N1		σ* (C5-C6)	0.0394	11.98	0.86	0.09
LP N1		σ* (C6-O8)	0.0490	5.74	0.74	0.06
LP O8	1.9623	σ* (N1-C6)	0.0271	7.86	1.11	0.08
LP N10	1.7013	π* (C2-C3)	0.4797	61.83	0.25	0.12
LP O18	1.9800	σ* (C3-N7)	0.0988	4.79	1.09	0.07
LP O19	1.9765	σ* (C3-N7)	0.0988	5.70	1.09	0.07

AMNP molecule, the ICT via the transitions between the lone pair to σ and σ* are responsible for the hydrogen bond formation and hyperconjugation interaction of the molecule [40]. These interactions lead to the higher stability of the AMNP molecule and are also listed in Table 6. The $\pi \rightarrow \pi^*$ transitions in the AMNP molecule account for the higher polarization identified. This polarization phenomenon is responsible for the NLO activity of the molecule [2, 4, 36].

4 Conclusion

The conformational analysis of the AMNP molecule has been carried out, and the three possible conformers of molecule are identified. The global minimum structure of the molecule was optimized based on the DFT/B3LYP method with 6-311G (d, p), 6-311++G (d,p), and cc-pVTZ basis sets. The optimized minimum energy molecular structure of the AMNP molecule predicted by the DFT/B3LYP method with cc-pVTZ basis set confirms the intramolecular hydrogen bond formation leading to the higher stability of the molecule. Mulliken atomic charge distribution analysis predicts the ICT interactions between the positive and negative atoms, indicating the formation of the intramolecular hydrogen bond. The vibrational spectral analysis has been carried out for the AMNP molecule. The observed and calculated vibrational frequencies are assigned on the basis of PED calculation. The UV–vis spectral analysis predicts the presence of *n*–π* and π–π* electronic transitions

in the AMNP molecule and are also confirmed theoretically using NBO analysis. The higher first-order hyperpolarizability value of the molecule confirms the NLO activity of the molecule. The FMOs analysis identifies the presence of delocalized electron density within the molecule and accounts for its higher reactivity. As the presence of intra-molecular interactions and the associated charge transfers between the pyridine ring of AMNP molecule and the lone pair of oxygen is a common molecular feature of a pharmaceutical compound, this investigation paves the way for its possible biomedical applications. Further, the considerably higher NLO activity of the molecule identified suggests its potential applications in the design of new optical materials.

Acknowledgments The authors thank the college management for encouragement and permission to carry out this work and also thank the Department of Physics, N.M.S.S.V.N.College, Nagamalai, Madurai-19, for providing the Gaussian 09 program package. The DST, New Delhi, and SAIF, IIT, Chennai shall be duly acknowledged for recording the FT-IR and FT-Raman spectra. This work was supported by the UGC Research Award scheme, New Delhi (F. no.30-35/2011 (SA-II)).

References

1. B. Machura, M. Wolff, Struct. Chem. **25**, 1607–1623 (2014)
2. S.G. Aziz, S.A. Elroby, A. Alyoubi, O.I. Osman, R. Hilal, J. Mol. Model. **20**, 2078 (2014)
3. S. Premkumar, A. Jawahar, T. Mathavan, M. Kumara Dhas, V.G. Sathe, A. Milton Franklin Benial, Spectrochim. Acta **129A**, 74–83 (2014)
4. S. Premkumar, A. Jawahar, T. Mathavan, M. Kumara Dhas, A. Milton Franklin Benial, Spectrochim. Acta **138A**, 252–263 (2015)
5. S. Tomaru, S. Matsumoto, T. Kurihara, H. Suzuki, N. Ooba, T. Kaino, Appl. Phys. Lett. **58**, 2583–2585 (1991)
6. W.S. Tang, X.X. Lu, K.M.C. Wong, V.W.W. Yam, J. Mater. Chem. **15**, 2714–2720 (2005)
7. N.O. Komatsuzaki, M. Yanagida, T. Funaki, K. Kasuga, K. Sayama, H. Sugihara, Sol. Energy Mater. Sol. Cells **95**, 310–314 (2011)
8. J. Lorenc, Vib. Spectrosc. **61**, 112–123 (2012)
9. O. Tamer, B. Sarıboğa, I. Uçar, Struct. Chem. **23**, 659–670 (2012)
10. I. Ajaj, J. Markovski, J. Marković, M. Jovanović, M. Milčić, F. Assaleh, A. Marinković, Struct. Chem. **25**, 1257–1270 (2014)
11. A.R. Nekoei, S.F. Tayyari, M. Vakil, J. Mol. Struct. **1075**, 85–95 (2014)
12. N.A. Sánchez-Bojorge, L.M. Rodríguez-Valdez, N. Flores-Holguín, J. Mol. Model. **19**, 3537–3542 (2013)
13. C. Ravikumar, I. Hubert Joe, Phys. Chem. Chem. Phys. **12**, 9452–9460 (2010)
14. I. Bryndal, E. Kucharska, W. Sasiadek, M. Wandas, T. Lis, J. Lorenc, J. Hanuza, Spectrochim. Acta **96A**, 952–962 (2012)
15. B.C. De Simone, A.D. Quartarolo, S. Cospito, L. Veltri, G. Chidichimo, N. Russo, Theor. Chem. Accounts **131**, 1225 (2012)
16. P. Hohenberg, W. Kohn, Phys. Rev. **136**, B864–B871 (1964)
17. A.D. Becke, J. Chem. Phys. **98**, 5648–5652 (1993)
18. C. Lee, W. Yang, R.G. Parr, Phys. Rev. B **37**, 785 (1988)
19. M.J. Frisch, G.W. Trucks, H.B. Schlegel, G.E. Scuseria, M.A. Robb, J.R. Cheeseman, J.A. Montgomery Jr., T. Vreven, K.N. Kudin, J.C. Burant, J. Millam, S.S. Iyengar, J. Tomasi, V. Barone, B. Mennucci, M. Cossi, G. Scalmani, N. Rega, G.A. Petersson, H. Nakatsuji, M. Hada, M. Ehara, K. Toyota, R. Fukuda, J. Hasegawa, M. Ishida, T. Nakajima, Y. Honda, O. Kitao, H. Nakai, M. Klene, X. Li, J.E. Knox, H.P. Hratchian, J.B. Cross, C. Adamo, J. Jaramillo, R. Gomperts, R.E. Stratmann, O. Yazyev, A.J. Austin, R. Cammi, C. Pomelli, J.W. Ochterski, P.Y. Ayala, K. Morokuma, G.A. Voth, P. Salvador, J.J. Dannenberg, V.G. Zakrzewski, S. Dapprich, A.D. Daniels, M.C. Strain, O. Farkas, D.K. Malick, A.D. Rabuck, K. Raghavachari, J.B. Foresman, J.V. Ortiz, Q. Cui, A.G. Baboul, S. Clifford, J. Cioslowski, B.B. Stefanov, G. Liu, A. Liashenko, P. Piskorz, I. Komaromi, R.L. Martin, D.J. Fox, T. Keith, M.A. Al-Laham, C.Y. Peng, A. Nanayakkara, M. Challacombe, P.M.W. Gill, B. Johnson, W. Chen, M.W. Wong, C. Gonzalez, J.A. Pople, *Gaussian 09, Revision C.02* (Gaussian Inc, Wallingford, 2009)
20. M.H. Jamroz, Vibrational energy distribution analysis VEDA 4.0 program, Warsaw. (2004)
21. R. Dennington, T. Keith, J. John Milam, GaussView, Version 5, Semichem Inc., Shawnee MissionKS. (2009)
22. E.D. Glendening, A.E. Reed, J.E. Carpenter, F. Weinhold, *NBO version 3.1, TCI* (University of Wisconsin, Madison, 1998)
23. T. Koopmans, Physica **1**, 104–113 (1934)
24. G. Keresztury, S. Holly, J. Varga, G. Besenyei, A.Y. Wang, J.R. Durig, Spectrochim. Acta **49A**, 2007 (1993)
25. D. Kheffache, H. Guemmour, A. Dekhira, A. Benaboura, O. Ouamerali, J. Mol. Model. **19**, 4837–4847 (2013)
26. H.F. Hameka, J.O. Jensen, J. Mol. Struct. (Theochem.) **362**, 325–330 (1996)
27. G. Socrates, *Infrared and raman characteristic group frequencies*, 3rd edn. (Wiley, New York, 2001)
28. G. Varsanyi, *Assignments for vibrational spectra of seven hundred benzene derivatives*, vol. 1 (Adam Hilger, London, 1974)
29. J.B. Lambert, H.F. Shurvell, D.A. Lightner, R.G. Cooks, Organic Struc. Spect, Simon & Schuster/A Viacom company, New Jersey. (1998)
30. D. Lin-vien, N.B. Cothup, W.G. Fateley, J.G. Graselli, *The handbook of infrared and raman characteristic frequencies of organic molecules* (Academic, Boston, 1991)
31. D. Arul Dhas, I. Hubert Joe, S.D. Dharma Roy, S. Balachandran, J. Mol. Model. **18**, 3587–3608 (2012)
32. H. Raissi, M. Yoosefian, F. Mollania, S. Khoshkhou, Struct. Chem. **24**, 123–137 (2013)
33. A.D. Khalaji, A.N. Chermahini, K. Fejfarova, M. Dusek, Struct. Chem. **21**, 153–157 (2010)
34. S. Şenay Yurdakul, S. Badoğlu, Struct. Chem. **20**, 423–434 (2009)
35. R.G. Parr, P.K. Chattaraj, J. Am. Chem. Soc. **113**, 1854–1855 (1991)
36. D. Manimaran, C. Jesintha John, V.K. Rastogi, I. Hubert Joe, Spectrochim. Acta **109A**, 173–178 (2013)
37. D.A. Kleinman, Phys. Rev. **126**, 1977–1979 (1962)
38. I. Fleming, *Frontier orbitals and organic chemical reactions* (Wiley, New York, 1976)
39. F. Weinhold, C.R. Landis, *Valency and bonding: a natural bond orbital donor-acceptor perspective* (Cambridge University Press, New York, 2005)
40. D.M. Suresh, M. Amalanathan, S. Sebastian, D. Sajan, I. Hubert Joe, V. Bena Jothy, I. Nemc, Spectrochim. Acta **115A**, 595–602 (2013)